Charge Localization in Isolated Mixed-Valence Complexes: An STM and Theoretical Study

Yuhui Lu,[†] Rebecca Quardokus,[‡] Craig S. Lent,[†] Frederic Justaud,[§]
Claude Lapinte,[§] and S. Alex Kandel*,[‡]

*Department of Electrical Engineering and Department of Chemistry and Biochemistry,
University of Notre Dame, Notre Dame, Indiana 46556, and Sciences Chimiques de Rennes,
Université de Rennes 1, UMR CNRS 6226, Campus de Beaulieu, F-35042 Rennes, France*

Received July 6, 2010; E-mail: skandel@nd.edu

Abstract: $\{Cp^*(dppe)Fe(C\equiv C-)\}_2(1,3-C_6H_4)$ is studied both as a neutral molecule, Fe(II)−Fe(II), and as a mixed-valence complex, Fe(II)−Fe(III). Scanning tunneling microscopy (STM) is used to image these species at 77 K under ultrahigh-vacuum conditions. The neutral molecule Fe(II)−Fe(II) has a symmetric, "dumbbell" appearance in STM images, while the mixed-valence complex Fe(II)−Fe(III) demonstrates an asymmetric, bright-dim double-dot structure. This asymmetry results from localization of the electron to one of the iron-ligand centers, a result which is confirmed through comparison to theoretical STM images calculated using constrained density-functional theory (CDFT). The observation of charge localization in mixed-valence complexes outside of the solution environment opens up new avenues for the control and patterning of charge on surfaces, with potential applications in smart materials and molecular electronic devices.

I. Introduction

Beginning with the work of Creutz and Taube[1,2] in 1969, there has been extensive research into the chemistry and physics of mixed-valence compounds. These molecular species have multiple oxidation−reduction (redox) centers, and electron transfer between these centers results in more than one energetically accessible electronic state for the molecule. These compounds are ideal candidates for the study of intramolecular electron and energy transfer.[3] Furthermore, mixed-valence complexes can be conductive and can exhibit significant nonlinear optical and magnetic properties, resulting in potential applications in molecular electronics.[4−6] The electronic properties of mixed-valence compounds strongly depend on the extent of the electronic interaction between the redox centers and range, in accordance with Robin−Day classification,[7] from small (class I), to slight (class II), to strong (class III) interactions. Various experimental techniques including observation of the intervalence transfer (IT) band,[8] electron spin resonance,[9] and ultraviolet photoelectron spectroscopy have been used to probe such interactions; there is also an extensive theoretical literature.[10,11]

In recent years, the investigation of the properties of isolated, individual molecules has been greatly facilitated by scanning tunneling microscopy (STM). STM has been used to study the adsorption site and geometry of molecules on surfaces,[12,13] to obtain high-resolution images of intramolecular structure,[14,15] to investigate the local electronic properties of individual molecules,[16−22] and to detect different spin states of transition-metal complexes.[23]

In this work, we use STM to observe charge localization within a mixed-valence complex. Each mixed-valence molecule has two electronic states which, in the isolated molecule, are degenerate: they have the same energy but are spatially distinct. Small perturbations in the environment mix these states to produce a highly asymmetric electron distribution, which can then be probed using STM. This is distinct from prior studies of intramolecular structure in that the local density of electronic states being probed is highly subject, qualitatively as well as

† Department of Electrical Engineering, University of Notre Dame.
‡ Department of Chemistry and Biochemistry, University of Notre Dame.
§ Université de Rennes 1.
(1) Creutz, C.; Taube, H. *J. Am. Chem. Soc.* **1969**, *91*, 3988.
(2) Creutz, C.; Taube, H. *J. Am. Chem. Soc.* **1973**, *95*, 1086.
(3) Hush, N. S.; Wong, A. T.; Bacskay, G. B.; Reimers, J. R. *J. Am. Chem. Soc.* **1990**, *112*, 4192.
(4) Aviram, A. *J. Am. Chem. Soc.* **1988**, *110*, 5687.
(5) Fraysse, S.; Coudret, C.; Launay, J.-P. *Eur. J. Inorg. Chem.* **2000**, *7*, 1581.
(6) Astruc, D. *Acc. Chem. Res.* **1997**, *30*, 383.
(7) Robin, M. B.; Day, P. *Adv. Inorg. Chem. Radiochem.* **1968**, *10*, 247.
(8) Hush, N. S. *Electrochim. Acta* **1968**, *13*, 1005.
(9) Rak, S. F.; Miller, L. L. *J. Am. Chem. Soc.* **1992**, *114*, 1388.
(10) Newton, M. D. *Chem. Rev.* **1991**, *91*, 767.
(11) Newton, M. D.; Cave, R. J. *Mol. Electron.* **1997**, 73.

(12) Chiang, S. *Chem. Rev.* **1997**, *97*, 1083.
(13) Han, P.; Mantooth, B. A.; Sykes, E. C. H.; Donhauser, Z. J.; Weiss, P. S. *J. Am. Chem. Soc.* **2004**, *126*, 10787.
(14) Weiss, P. S.; Eigler, D. M. *Phys. Rev. Lett.* **1993**, *71*, 3139.
(15) Qiu, X. H.; Nazin, G. V.; Ho, W. *Science* **2003**, *299*, 542.
(16) Pascual, J. I.; Jackiw, J. J.; Song, Z.; Weiss, P. S.; Conrad, H.; Rust, H. P. *Surf. Sci.* **2002**, *502*, 1.
(17) Lei, S. B.; Deng, K.; Yang, D. L.; Zeng, Q. D.; Wang, C. *J. Phys. Chem. B* **2006**, *110*, 1256.
(18) Lu, X.; Hipps, K. W.; Wang, X. D.; Mazur, U. *J. Am. Chem. Soc.* **1996**, *118*, 7197.
(19) Lu, X.; Grobis, M.; Khoo, K. H.; Louie, S. G.; Crommie, M. F. *Phys. Rev. Lett.* **2003**, *90*, 096802.
(20) Kirczenow, G.; Piva, P. G.; Wolkow, R. A. *Phys. Rev. B* **2009**, *80* (33), 035309.
(21) Haider, M. B.; Pitters, J. L.; DiLabio, G. A.; Livadaru, L.; Mutus, J. Y.; Wolkow, R. A. *Phys. Rev. Lett.* **2009**, *102*, 046805.
(22) Baber, A. E.; Jensen, S. C.; Sykes, E. C. H. *J. Am. Chem. Soc.* **2007**, *129* (20), 6368.
(23) Alam, M. S.; Stocker, M.; Gieb, K.; Müller, P.; Haryono, M.; Student, K.; Grohmann, A. *Angew. Chem., Int. Ed.* **2010**, *49*, 1159–1163.

quantitatively, to the specific nature of the molecule's local environment, and changes in the environment could potentially make this charge distribution dynamic and manipulatable.

Our interest in the dynamic redistribution of intramolecular charge was prompted initially by our long-standing interest in molecular electronics and quantum-dot cellular automata (QCA).[24-26] QCA is a paradigm for nanoelectronics, in which binary information is encoded in charge configuration of a QCA cell and transferred via Coulomb interaction between neighboring cells. Metal-based[27] and semiconductor-based[28,29] QCA cells have been fabricated, and information encoding and transfer have been demonstrated at cryogenic temperatures.[30] At the molecular scale, each QCA cell can potentially be realized by a mixed-valence molecule, and different molecular charge configurations can then be used to represent binary information. Several candidate molecules have been synthesized,[31-33] and we have obtained STM images of one such candidate in our previous studies.[34-36]

Another motivation for this work is to understand the physics and chemistry of mixed-valence molecules that are adsorbed on surfaces. This is a departure from traditional experimental and theoretical approaches, which have exclusively looked at mixed-valence molecules in solution. Solvent organization plays a large and, in many cases, dominant role in determining electron-transfer kinetics in these cases. The current STM investigation enables us to explore the properties of single, isolated mixed-valence molecules in the absence of solvent. These properties include the oxidation state, electron transfer rates, and surface screening, all of which are important for the incorporation of mixed-valence molecules into molecular-electronic devices as well as other structured, heterogeneous materials.

Here we report an STM investigation of $\{Cp^*(dppe)Fe(C\equiv C-)\}_2(1,3\text{-}C_6H_4)$,[37-39] referred to as Fe2; the molecular structure is shown in Figure 1. We choose this molecule because of its chemical stability and the weak coupling between the two metal centers. Fe2$^+$ was identified as a type II mixed-valence complex according to the Robin−Day classification. The electron transfer matrix element, which measures the coupling between the two redox centers, is approximately 0.02 eV.[39] This weak coupling
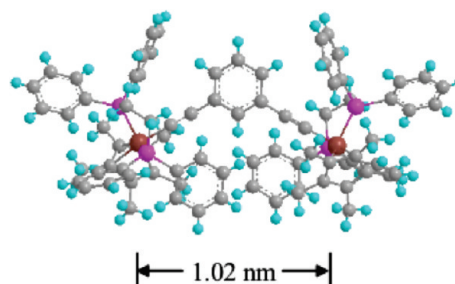

Figure 1. The structure of Fe2, $\{Cp^*(dppe)Fe(C\equiv C-)\}_2(1,3\text{-}C_6H_4)$. Two Cp*(dppe)Fe− moieties function as two quantum dots. For the mixed valence complex, the mobile electron can localize on one site or the other. The bistable charge configuration is the foundation for using mixed-valence complex as QCA cells.

between two Fe atoms enables the charge localization on one site or the other, resulting in Fe(II)Fe(III) or Fe(III)Fe(II) configurations.

II. Experimental and Theoretical Methodology

The dinuclear complex molecule used in this investigation, $\{Cp^*(dppe)Fe(C\equiv C-)\}_2(1,3\text{-}C_6H_4)$ (hereafter denoted as molecule Fe2), was synthesized by Lapinte and co-workers.[37-39] (It is described in ref 38 as molecule **2**.) This molecule contains two Cp*(dppe)Fe moieties connected via a phenylene ring, as shown in Figure 1. Fe2 solutions are made by dissolving Fe2 in THF inside a argon-purged glovebox. The mixed-valence Fe2$^+$ is made by mixing Fe2 with ferrocenium hexafluorophosphate ([Fe(η^5-$C_5H_5)_2$][PF$_6$]) in a 1:1 mol ratio in either THF, toluene, or dichloromethane

$$Fe2 + [Fe(\eta^5\text{-}C_5H_5)_2][PF_6] \rightarrow [Fe2]^+[PF_6]^- + Fe(\eta^5\text{-}C_5H_5)_2$$
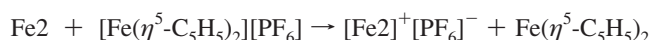
Fe2 is a neutral dinuclear complex with both Fe atoms in the +2 valence state. For the mixed-valence Fe2$^+$, one of the Fe atoms is oxidized to a +3 valence state, resulting in an odd electron that can tunnel between two Fe centers through the 1,3-C$_6$H$_4$ linker. The localization of this mobile electron results in either the Fe(II)−Fe(III) or the Fe(III)−Fe(II) configuration.

The sample used for STM imaging is prepared by the pulse-deposition technique. This technique was developed by Kawai and co-workers[40] to deposit high-molecular-weight, reactive molecules that are not compatible with thermal evaporation methods. In our previous studies, we have used the pulse-deposition technique to deposit dinuclear ruthenium-based compounds onto a gold surface.[34,35] In this work, commercial Au(111)-on-mica samples (Agilent Technologies) were used as substrates for the deposition of target molecules. The Au substrates were sputtered and annealed before Fe2 deposition, with argon sputtering at 500 eV ion energy and 20 μA ion current, followed by annealing at 700−800 K. Two or three cycles (15 min of sputtering followed by 30 min of annealing) produced clean, crystalline Au(111) surfaces for subsequent Fe2 deposition. The clean Au(111) was transferred to a load-lock chamber with a pulsed valve (Parker Instrumentation 9-series, 0.5 mm nozzle diameter, IOTA One driver) installed. Typically, two or three pulses of 2 ms duration were used to inject solution onto the surface. The sample was then imaged at liquid-nitrogen temperature using a low-temperature UHV STM (Omicron Nanotechnology LT-STM) in constant-current mode. The base pressure of the STM chamber was kept in the 10^{-10} Torr range during measurements.

Calculating the electronic structures of transition-metal-containing mixed-valence complexes is challenging, and it is particularly

(24) Lent, C. S.; Tougaw, P. D.; Porod, W.; Bernstein, G. H. *Nanotechnology* **1993**, *4*, 49.
(25) Lent, C. S. *Science* **2000**, *288*, 1597.
(26) Tougaw, P. D.; Lent, C. S. *J. Appl. Phys.* **1994**, *75*, 1818.
(27) Orlov, A. O.; Amlani, I.; Bernstein, G. H.; Lent, C. S.; Snider, G. L. *Science* **1997**, *277*, 928.
(28) Perez-Martinez, F.; Farrer, I.; Anderson, D.; Jones, G. A. C.; Ritchie, D. A.; Chorley, S. J.; Smith, C. G. *Appl. Phys. Lett.* **2007**, *91*, 032102.
(29) Mitic, M.; Cassidy, M. C.; Petersson, K. D.; Starrett, R. P.; Gauja, E.; Brenner, R.; Clark, R. G.; Dzurak, A. S. *Appl. Phys. Lett.* **2006**, *89*, 013503.
(30) Amlani, I.; Orlov, A. O.; Toth, G.; Bernstein, G. H.; Lent, C. S.; Snider, G. L. *Science* **1999**, *284*, 289.
(31) Qi, H.; Sharma, S.; Li, Z.; Snider, G. L.; Orlov, A. O.; Lent, C. S.; Fehlner, T. P. *J. Am. Chem. Soc.* **2003**, *125*, 15250.
(32) Jiao, J.; Long, G. J.; Rebbouh, L.; Grandjean, F.; Beatty, A. M.; Fehlner, T. P. *J. Am. Chem. Soc.* **2005**, *127*, 17819.
(33) Qi, H.; Gupta, A.; Noll, B. C.; Snider, G. L.; Lu, Y.; Lent, C. S.; Fehlner, T. P. *J. Am. Chem. Soc.* **2005**, *127*, 15218.
(34) Wei, Z.; Guo, S.; Kandel, S. A. *J. Phys. Chem. B* **2006**, *110*, 21846.
(35) Guo, S.; Kandel, S. A. *J. Chem. Phys.* **2008**, *128* (1), 014702.
(36) Guo, S.; Kandel, S. A. *J. Phys. Chem. Lett.* **2010**, *1*, 420.
(37) Weyland, T.; Lapinte, C.; Frapper, G.; Calhorda, M. J.; Hartlet, J.-F.; Toupet, L. *Organometallics* **1997**, *16*, 2024.
(38) Weyland, T.; Costuas, K.; Mari, A.; Halet, J.-F.; Lapinte, C. *Organometallics* **1998**, *17*, 5569.
(39) Weyland, T.; Costuas, K.; Toupet, L.; Halet, J.-F.; Lapinte, C. *Organometallics* **2000**, *19*, 4228.

(40) Kanno, T.; Tanaka, H.; Nakamura, T.; Tabata, H.; Kawai, T. *Jpn. J. Appl. Phys.* **1999**, *38*, L606.

difficult to predict the charge localization correctly. Normally a multiple-configurational self-consistent field (MCSCF) method[41] is needed to obtain an accurate electronic structure of a donor−acceptor electron transfer system, but a full MCSCF calculation is extremely expensive for transition-metal-containing mixed-valence complexes like Fe2. The single-determinant Hartree−Fock (HF) method is computationally more tractable, yet it lacks accuracy and tends to overestimate charge localization. Density functional theory (DFT) can treat large molecules with reasonable accuracy and is extensively employed for the transition-metal-containing systems, but recent studies show that DFT methods dramatically fail to capture electron localization: the mobile electron tends to delocalize over the donor and acceptor groups, and the donor−acceptor interactions are usually overestimated.[42] The origin of this failure is attributed to the delocalization error of the exchange-correlation functional as well as the self-interaction error.[43]

In the current study, we use constrained density functional theory (CDFT) to investigate the electronic structure of Fe2 molecule. The CDFT method was first suggested by Dederichs et al.[44] and more recently developed by Wu and Van Voorhis.[45−47] This method is based on the traditional density functional theory of Hohenberg, Kohn, and Sham,[48] but with the additional requirement that ground-state electron density satisfies some special constraint. CDFT has been successfully applied to study electron transfer in systems with large molecules containing transition metals. When applied to mixed-valence complexes, the CDFT constraint requires the mobile electron to localize on either the donor site or the acceptor site.[45−47]

III. Results

Figure 2 shows STM images of isolated Fe2 molecules on the Au(111) surface. Bright, paired, circular features with an apparent height of 3 Å are distributed over the imaged area, and we assign each dumbbell-shaped feature to an Fe2 molecule. The distance between circles within each dumbbell is 1 nm, which is consistent with this assignment. The intramolecular axis is apparently randomly oriented in the surface plane, which suggests a relatively smooth molecule-surface potential; the observation of molecules with different orientations also rules out the possibility of tip-convolution artifacts in these images.

Two areas of Figure 2(a) are enlarged in Figures 2(c) and 2(d). We propose that the molecules are lying flat, with their long axes parallel to the surface. (This is further confirmed by theoretical calculations, which will be discussed presently.) This configuration is similar to earlier measurements in our lab of ruthenium-based complexes. Each bright feature corresponds to one Cp*(dppe)Fe− moiety. The two Cp*(dppe)Fe− moieties are clearly resolved in the STM images, but the internal (C≡C−)}$_2$(1,3-C$_6$H$_4$) linker is invisible with the imaging conditions used here. A molecular structure of Fe2, drawn to scale, is presented in the inset of Figure 2(c); as the STM is independently calibrated, there are no adjustable parameters involved in this comparison. The good agreement between the STM image and the molecular geometry supports our assignment that each paired-dot structure is a single Fe2 molecule.

Smaller and dimmer features visible in the background of Figure 2 result from solvent (toluene) molecules that remain
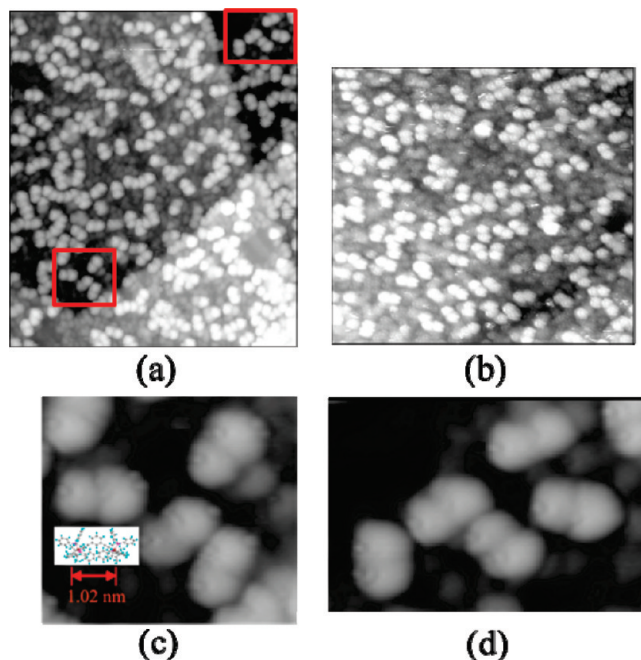

Figure 2. (a) 460 Å × 520 Å STM images of Fe2 molecules on Au(111) at 77 K, acquired at 0.5 V sample bias and 20 pA tunneling current; (b) 371 Å × 405 Å STM images of Fe2 molecules on Au(111) at 77 K, acquired at 0.5 V sample bias and 20 pA tunneling current; (c, d) enlarged images of two areas framed in panel (a). For all the above images, the dot−dot distance is about 1 nm, which is in good agreement with Fe−Fe distance.
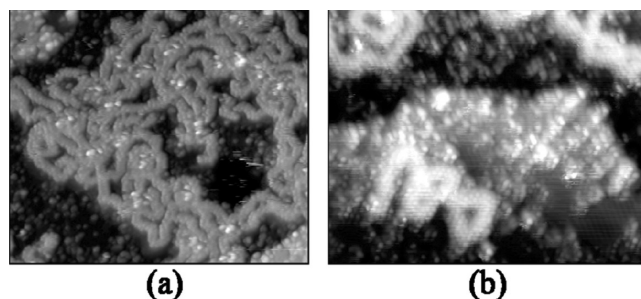

Figure 3. (a) 289 Å × 341 Å STM images of Fe2$^+$ mixed valence in THF on Au(111); (b) 211 Å × 267 Å STM images of FcPF$_6$ plus dichloromethane on Au(111).

on the surface after pulse deposition. To avoid any possible decomposition of Fe2, no postdeposition annealing step is used, but the presence of residual solvent cannot then be avoided.[16] Additional species are present in solution for investigation of Fe2$^+$ samples: FcPF$_6$ is used to oxidize Fe2 to Fe2$^+$, and the solutions used to deposit Fe2$^+$ will contain solvent, unreacted ferrocenium, ferrocene, unoxidized Fe2, and Fe2$^+$. We observe distinctive, labyrinthine features in samples exposed only to THF and FcPF$_6$, with a representative image shown in Figure 3b, which shows an image of a blank experiment without Fe2 and Fe2$^+$. These features may be formed due to the electrostatic interaction between cations and anions, but the mechanism remains unknown due to the complex kinetics resulting from changes in concentration and temperature during pulse deposition.

Figure 4 shows isolated single-molecule images of mixed-valence Fe2$^+$, where molecules can be seen clearly among the features resulting from THF and FcPF$_6$. The framed double-dot features in Figure 4 are assigned as the images of individual Fe2$^+$ molecules. Comparing Figure 4 and Figure 2, the differences between the mixed-valence and neutral molecules are

(41) Yamamoto, N.; Vreven, T.; Robb, M. A.; Frisch, M. J.; Schlegel, H. B. *Chem. Phys. Lett.* **1996**, *250*, 373.
(42) Lu, Y.; Lent, C. S. *Nanotechnology* **2008**, *19*, 155703.
(43) Cohen, A. J.; Mori-Sánchez, P.; Yang, W. *Science* **2008**, *321*, 792.
(44) Dederichs, P. H.; Blügel, S.; Zeller, R.; Akai, H. *Phys. Rev. Lett.* **1984**, *53*, 2512.
(45) Wu, Q.; Van Voorhis, T. *Phys. Rev. A* **2005**, *72*, 024502.
(46) Wu, Q.; Van Voorhis, T. *J. Chem. Theory Comput.* **2006**, *2*, 765.
(47) Wu, Q.; Van Voorhis, T. *J. Phys. Chem. A* **2006**, *110*, 9212.
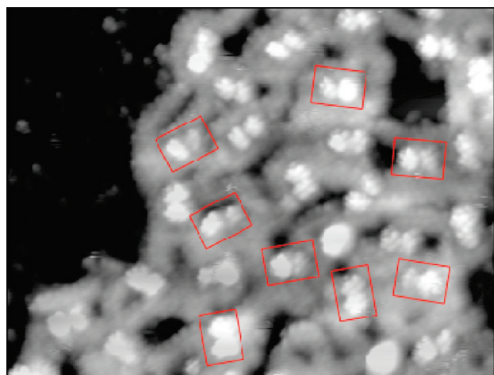(48) Hohenberg, P.; Kohn, W. *Phys. Rev.* **1964**, *136* (3B), B864.

Figure 4. 230 Å × 170 Å STM images of oxidized Fe2 sample on Au(111) at 77 K, acquired at 1 V sample bias and 5 pA tunneling current. The framed areas are assigned as images of mixed-valence complexes Fe2$^+$. The bright-dim double-dot structures demonstrate the uneven charge distribution. The mobile charge localizes on one site or the other.

Table 1. Selected Optimized Bond Length (Å) for the Model Molecules Cp(PH$_3$)$_2$Fe(C≡C−C$_6$H$_5$)$^{n+}$ (Fe1-H^{n+}; n = 0, 1) and {Cp(PH$_3$)$_2$Fe(C≡C−)}$_2$(1,3-C$_6$H$_4$)$^+$ (Fe2-H$^+$)

	1-H(DFT)	1-H$^+$(DFT)	2-H$^+$(DFT)	2-H$^+$(CDFT)
Fe1−C$_\alpha$1	1.921	1.857	1.872	1.914
Fe2−C$_\alpha$2			1.872	1.873
C$_\alpha$1−C$_\beta$1	1.225	1.233	1.233	1.226
C$_\alpha$2−C$_\beta$2			1.233	1.226
C$_\beta$1−C1	1.426	1.414	1.412	1.423
C$_\beta$2−C3			1.412	1.422
Fe1−P$_\alpha$1	2.212	2.262	2.230	2.213
Fe1−P$_\beta$1	2.212	2.264	2.230	2.215
Fe1−Cp	1.757	1.774	1.761	1.760
Fe2−P$_\alpha$2			2.230	2.278
Fe2−P$_\beta$2			2.230	2.287
Fe2−Cp			1.761	1.777

Scheme 1

1-H

2-H

readily apparent in STM images. While the double-dot feature of neutral Fe2 appears symmetric, mixed-valence Fe2$^+$ (prepared as Fe$_2$$^+PF_6$$^-$ in solution by oxidation with FcPF$_6$) appears with one metal center distinctly brighter than the other. Similar contrasts between oxidized and unoxidized moieties have been observed on mixed-valence Ru2 molecules that we have reported previously.[36] For this study, many aspects of surface and sample preparation are identical for both the neutral and mixed-valence samples. Differences in the composition of the sample are largely addressed by the control experiments described. Therefore, the most straightforward explanation of the asymmetry that is observed only for the molecules in the mixed-valence sample is that charge indeed remains localized on one side of the molecule. This interpretation gains further support from the results of our DFT calculations.

Theoretical calculations are conducted using the constrained DFT (CDFT) method.[45−47] We use CDFT to calculate the electron density of an Fe2 molecule subject to an imposed constraint: a positive unit charge must remain on one of the two Cp(PH$_3$)$_2$Fe(C≡C−) moieties. Electronic asymmetry is therefore forced in this calculation, and the purpose of the calculation is the prediction of STM images that would result from such an asymmetric charge distribution. The strong qualitative agreement that we observe between experiment and theory tells us that charge localization could indeed result in the molecular features we observe, and that our images are consistent with the presence of mixed-valence molecules adsorbed on the surface.
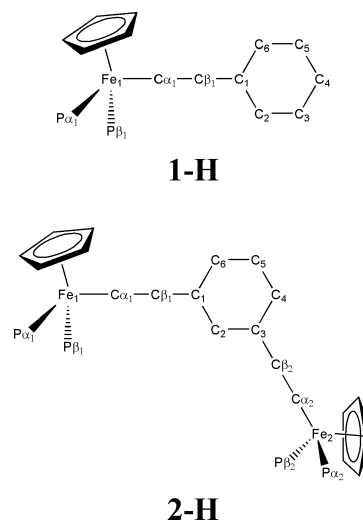
The B3LYP exchange-correlation potential is employed in the CDFT calculation. 6-311G** basis sets are used for C, H, and P atoms, and the ECP basis LANL2TZ(f) is used for Fe atoms. To reduce computational effort, we replace the bidentate dppe ligand with pairs of hydrogen-terminated phosphorus atoms, (PH$_3$)$_2$ and thus model {Cp*(dppe)Fe(C≡C−)}$_2$(1,3-C$_6$H$_4$) (Fe2) and {Cp*(dppe)Fe(C≡C−)}$_2$(1,3-C$_6$H$_4$)$^+$ (Fe2$^+$) by {Cp(PH$_3$)$_2$Fe(C≡C−)}$_2$(1,3-C$_6$H$_4$) (Fe2-H) and {Cp(PH$_3$)$_2$Fe(C≡C−)}$_2$(1,3-C$_6$H$_4$)$^+$ (Fe2-H$^+$), respectively, as previous studies did.[39] Charge density is constrained such that a positive unit charge is localized on one Cp(PH$_3$)$_2$Fe(C≡C−) moiety. We recognize that a fully quantitative comparison between calculated and experimental STM images would require an optimization of exact amount and location of charge, using the full ligand.[47]

We optimized the geometries of Fe1-H, Fe1-H$^+$, and Fe2-H$^+$. Fe1-H and Fe1-H$^+$ were optimized for comparison. Fe2-

H$^+$ was optimized using both conventional DFT and constrained DFT. A subset of the geometrical parameters is given in Table 1. The difference between Fe1-H and Fe1-H$^+$ is obvious: the Fe−C$_\alpha$ separations differ by 0.064 Å (Fe−C$_\alpha$ = 1.921 Å for Fe1-H and 1.857 Å for Fe1-H$^+$, see Scheme 1 for atom numbering). The average bond length of Fe−P differs by 0.051 Å, and Fe−Cp distances differ by 0.017 Å. This geometrical difference is obviously caused by the different oxidation state. Since Fe2$^+$ is a weakly coupled mixed-valence complex, one expects the geometry of Fe2-H$^+$ to show strong asymmetry, with one Cp(PH$_3$)$_2$Fe(C≡C−) having a similar geometry to Fe1-H and the other Fe1-H$^+$. However, the conventional DFT optimization fails to produce this difference. As can be seen from Table 1, the geometry of Fe2-H$^+$ is almost symmetrical, with the two Cp(PH$_3$)$_2$Fe(C≡C−) moieties having identical geometric parameters. This is because the conventional DFT overestimates charge delocalization: the mobile electron is forced to delocalize over the whole molecule under the conventional DFT calculation, even though the donor/acceptor coupling is rather weak in our case. The root of this failure is the self-interaction error of conventional DFT methods.[43]

The geometry of the two Cp(PH$_3$)$_2$Fe(C≡C−) moieties differs noticeably according to the constrained DFT optimization. For example, the Fe−C$_\alpha$ separations differ by 0.041 Å (Fe$_1$−C$_{\alpha 1}$ = 1.914 and Fe$_2$−C$_{\alpha 2}$ = 1.873). The average bond length of Fe−P differs by 0.069 Å, and Fe−Cp distances differ by 0.017 Å. The perceptible geometrical differences between two Fe-containing redox centers are in agreement with the fact that Fe2$^+$
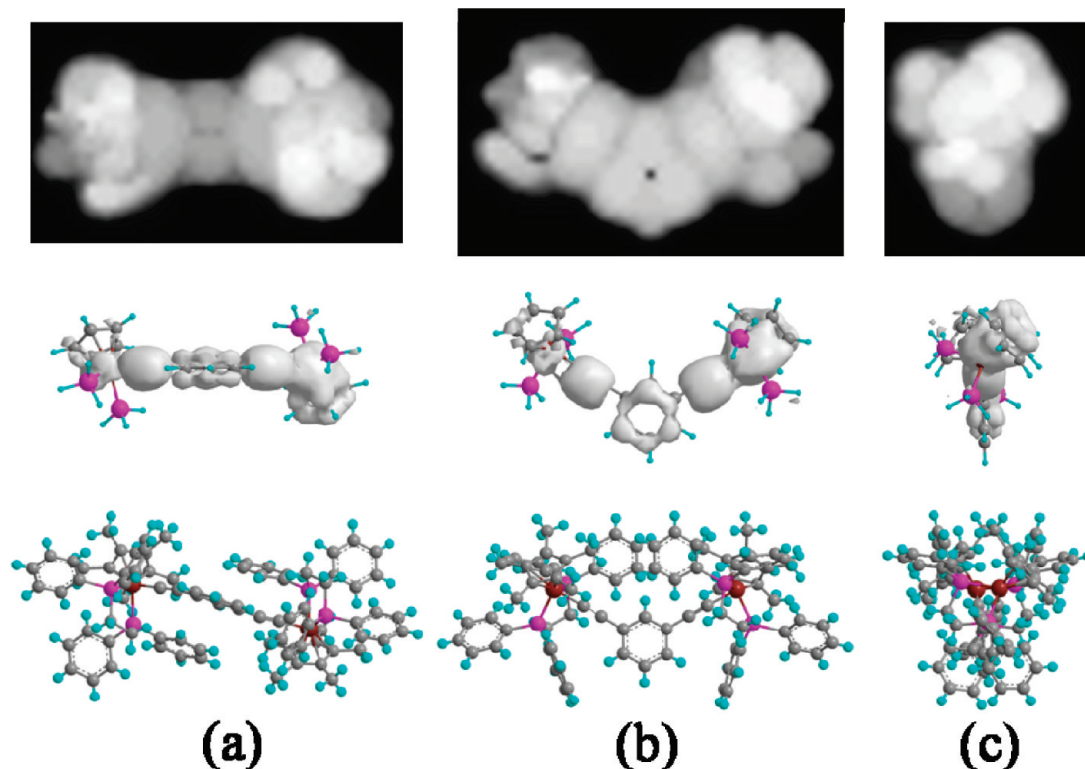
Figure 5. Simulated STM images, LDOS of the highest five occupied orbitals, and different views of molecule $Fe2^+$ along x, y, and z directions.

is a type II Robin−Day mixed-valence complex: the mobile electron is localized on one site instead of delocalizing over the entire molecule. It is the nuclear relaxation induced by charge localization that gives the geometrical difference between donor and acceptor.

To calculate theoretical STM images of the mixed-valence Fe2 molecule, we adopted Tersoff and Hamann's formula.[49] In this method, the STM tunneling-current can be expressed as

$$I(V) \propto \int_{E_f}^{E_f + eV} \rho(\vec{r}, E)\, dE$$

$$\rho(\vec{r}, E) = \sum_i |\Psi_i(\vec{r})|^2 \delta(E - E_i)$$

where $\rho(\vec{r}, E)$, $\Psi_i(\vec{r})$ and E_f are, respectively, the local density of states (LDOS) of the sample, the sample wave function with energy E_i and the Fermi level. The above equations assume a constant density of states of the tip, which allow us to obtain STM images from only the LDOS of the sample surface. We obtain the LDOS by summing the square of the eigenvectors within the energy range from E_f to $E_f + eV$, where V in theory is bias voltage of the sample relative to STM tip in experiment. In this work, because our computation is carried out on model molecule $Fe2\text{-}H^+$ instead of $Fe2^+$, V is difficult to determine precisely. We calculate the LDOS by including the highest five occupied orbitals.

Figure 5 shows simulated STM images of Fe2-H+ on three different projected directions. The LDOS is integrated over the x, y, and z directions, respectively, and a constant-current image is simulated by calculating the topography of a surface of constant integrated LDOS. Figure 5(a) corresponds to the predicted STM image when the molecule is lying flat, with the plane of the $-(C_6H_4)-$ linker perpendicular to the surface.

Figure 5(b) is the image when the molecule is lying flat, but the $-(C_6H_4)-$ linker parallel to the surface. Figure 5(c) is the image when two Fe-centered moieties align along the surface normal. Compared with Figure 4, Figure 5(a) is consistent with the experimental results. The dominant contributions of two Fe-containing redox groups result in a dumbbell shape. Since the double-dot dumbbell shape is clearly seen, and the $-(C_6H_4)-$ linker is invisible from the experimental STM image, we believe Fe2 molecules are lying flat, with the $-(C_6H_4)-$ linker perpendicular to the surface. Due to the uneven charge distribution, one redox group is brighter, and the other is dimmer.

IV. Discussion

Our simulated STM image qualitatively reproduces the experimental results. For the mixed-valence complex $Fe2^+$, both experimental and computational studies demonstrate that one side of the molecule is brighter than the other due to the charge localization. The geometrical optimization also suggests the asymmetrical nature of the two Fe-centered moieties. We attribute the computational success to the unique algorithm of constrained DFT, which maintains the accuracy of conventional DFT, and allows the mobile electron to localize on the donor/acceptor site. While charge localization here is achieved by algorithmic construction, the comparison to experiment indicates that the full charge is indeed localized on one side of the molecule. This is consistent with the physical reality that $Fe2^+$ has a weak coupling ($V_{ab} = 0.02$ eV) between two metal centers, which was established by the intervalence charge transfer band measurement.[39] We believe the constrained DFT method is a helpful tool to understand the charge transfer problem in complicated molecular systems, where the more sophisticated MCSCF methods are not practical and conventional DFT fails to reproduce the charge localization.

(49) Tersoff, J.; Hamann, D. R. *Phys. Rev. B* **1985**, *31* (2), 805.

In this work, STM images of both the neutral and the mixed-valence Fe2 molecule are obtained using ultrahigh-vacuum STM at cryogenic temperatures. The isolated molecules are clearly observed with submolecular, "dumbbell" structure evident in high-resolution STM images. For the neutral species, the two sides of the molecule are identical, which demonstrates the symmetric, uniform distribution of charge between the two iron groups; on the contrary, the mixed-valence species shows an asymmetrical double-dot structure, which reflects the localized, bistable configuration of the type II mixed-valence Fe(II)−Fe(III)/Fe(III)−Fe(II). The fact that STM images of mixed-valence complex $Fe2^+$ can recognize the different oxidation state of two Fe moieties is critical for implementing mixed-valence complexes as binary information encoder. One of the challenges of realizing molecular electronics is to "set" the input and "read" the output signal at the single molecular level. The above observation suggests STM can observe the molecular electronic structure directly. This enables us to "read" the logic value of molecular electronic devices. Future work will include manipulating neighboring molecules to fabricate various simple devices and demonstrate their logic function. In our current experiments,

conditions are kept so that the STM tip perturbs the sample as little as possible, and proposed manipulation experiments are particularly challenging for this system, as closer proximity between the tip and sample tends to result in the transfer of weakly bound adsorbates (solvent, Fe2, ferrocenium) onto the tip. We are working to address these challenges.

To our knowledge, this is the first reported measurement of a single, isolated, mixed-valence molecule probed outside of the solution environment, as well as the first calculation of an STM image using constrained density functional theory. STM imaging allows the electronic density of states of these molecules to be probed directly, and the results of this measurement can be compared to electronic structure calculated *ab initio*. Constrained density functional theory provides a computationally tractable method for theoretical modeling of mixed-valence, transition-metal-containing molecules, and the agreement with experimental results is strong.

JA105958P